Accumulation of Multiple Intermediates in the Catalytic Cycle of (4-Hydroxyphenyl)pyruvate Dioxygenase from *Streptomyces avermitilis*†

Kayunta Johnson-Winters, Vincent M. Purpero, Michael Kavana, and Graham R. Moran*

Department of Chemistry and Biochemistry, University of Wisconsin−Milwaukee, 3210 North Cramer Street, Milwaukee, Wisconsin 53211-3029

Received November 9, 2004; Revised Manuscript Received March 29, 2005

ABSTRACT: (4-Hydroxyphenyl)pyruvate dioxygenase (HPPD) catalyzes the conversion of (4-hydroxyphenyl)pyruvate (HPP) to homogentisate (HG). This reaction involves decarboxylation, substituent migration, and aromatic oxygenation in a single catalytic cycle. HPPD is a unique member of the α-keto acid dependent oxygenases that require Fe(II) and an α-keto acid substrate to oxygenate or oxidize an organic molecule. We have examined the reaction coordinate of HPPD from *Streptomyces avermitilis* using rapid mixing pre-steady-state methods in conjunction with steady-state kinetic analyses. Acid quench reactions and product analysis of homogentisate indicate that HPPD as isolated is fully active and that experiments limited in dioxygen concentration with respect to that of the enzyme do involve a single turnover. These experiments indicate that during the course of one turnover the concentration of homogentisate is stoichiometric with enzyme concentration by ∼200 ms, well before the completion of the catalytic cycle. Subsequent single turnover reactions were monitored spectrophotometrically under pseudo-first-order and matched concentration reactant conditions. Three spectrophotometrically distinct intermediates are observed to accumulate. The first of these is a relatively strongly absorbing species with maxima at 380 and 480 nm that forms with a rate constant (k_1) of 7.4×10^4 M^{-1} s^{-1} and then decays to a second intermediate with a rate constant (k_2) of 74 s^{-1}. The rate constant for the decay of the second intermediate (k_3) is 13 s^{-1} and is concomitant with the formation of the product, homogentisate, based on rapid quench and pre-steady-state fluorescence measurements. The rate constant for this process decreases to 7.6 s^{-1} when deuterons are substituted for protons in the aromatic ring of the substrate. The release of product from the enzyme is rate limiting and occurs at 1.6 s^{-1}. This final event exhibits a kinetic isotope effect of 2 with deuterium oxide as the solvent, consistent with a solvent isotope effect on V_{max} of 2.6 observed in steady-state experiments.

(4-Hydroxyphenyl)pyruvate dioxygenase (HPPD)[1] is a non-heme Fe(II)-dependent enzyme that catalyzes the conversion of (4-hydroxyphenyl)pyruvate (HPP) to homogentisate (HG) in the tyrosine catabolism pathway (Scheme 1). Continued scientific interest in HPPD has arisen from the importance of this enzyme in the treatment of type 1 tyrosinemia and alkaptonuria and also as a target for the development of herbicides (*1*−*4*). When classified according to the reaction catalyzed, HPPD belongs to a family of Fe(II)-dependent oxygenases that require both an α-keto acid, typically α-ketoglutarate (AKG), and molecular oxygen in order to hydroxylate or oxidize a third substrate. The paradigm examples of enzymes in this class include taurine dioxygenase (TauD), proline hydroxylase, deacetoxycepholsporin C synthase, and clavaminate synthase (*5*−*7*). Both HPPD and hydroxymandelate synthase are the known exceptions within this family as both of these enzymes have only two substrates, HPP and molecular oxygen. The required α-keto acid moiety is from the pyruvate substituent of HPP, and therefore, these enzymes do not require α-ketoglutarate (*8*, *9*).

Scheme 1

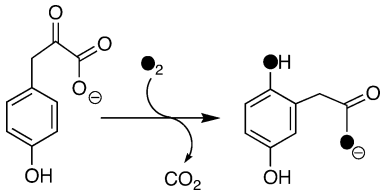

The reaction that α-keto acid dependent enzymes catalyze consists of one atom of dioxygen being added at the α-keto carbon to form a new carboxylic acid moiety and displace carbon dioxide and the other atom being incorporated as a hydroxyl or reduced to water. Bidentate binding of the α-keto acid substrate to the active site ferrous ion is a partial requirement for catalysis, and oxygen reactivity is heightened only in the presence of all organic substrates (*9*−*14*). A number of plausible mechanisms for the ensuing events of catalysis have been published (*15*−*18*); however, with one noteworthy exception, the chemical mechanism for α-keto acid dependent enzymes is largely unsupported by data that

† This research was supported by National Institutes of Health Grant DK59551 to G.R.M.

* To whom correspondence should be addressed. Tel: 414-229-5031. Fax: 414-229-5530. E-mail: moran@uwm.edu.

[1] Abbreviations: HEPES, *N*-(2-hydroxyethyl)piperazine-*N*′-2-ethanesulfonic acid; HPPD, (4-hydroxyphenyl)pyruvate dioxygenase; HPP, (4-hydroxyphenyl)pyruvate; HG, (2,5-dihydroxyphenyl)acetate; TAT, tyrosine aminotransferase; SDS, sodium dodecyl sulfate; PAGE, polyacrylamide gel electrophoresis; TCA, trichloroacetic acid; AKG, α-ketoglutarate; PLP, pyridoxal 5′-phosphate.

10.1021/bi047625k CCC: $30.25
Published on Web 04/23/2005

provide evidence for the accumulation and/or identity of catalytic intermediates.

It has been shown that the complex of an α-keto acid dependent enzyme with an α-keto acid produces a number of weak metal-to-ligand charge transfer transitions (*9*, *16*, *17*, *19*, *20*). In recent years this weak chromophore has been exploited as a visible spectrophotometric reporter to measure substrate binding constants and in rapid mixing pre-steady-state analyses to determine catalytic rate constants with TauD and HPPD (*9*, *17*, *21*). For TauD, a combination of spectrophotometric and freeze quench, rapid mixing methodologies revealed an Fe(IV) intermediate that accumulates prior to oxygenation of taurine (*16*, *22*−*24*). The definitive observation of an Fe(IV) intermediate was a significant advance in the study of α-keto acid dependent enzymes and is clearly at the frontier of future elucidation of mechanism.

Thorough spectrophotometric pre-steady-state analyses of any enzyme can assist the definitive chemical identification of intermediates. Such methods establish the time frame in which intermediates accumulate and decay, and the measured rate constants permit the determination of fractional accumulation of each transient at a given point in time. These data can thus be used to assist the analysis of subsequent static physical data for mixtures of trapped intermediate states. To date, the only pre-steady-state mechanistic evidence for HPPD was the observation of the accumulation of an intermediate with absorbance at 490 nm (*9*). Here, we present a more comprehensive analysis of the primary rate-limiting events in a single catalytic cycle of HPPD and provide evidence for the accumulation of three intermediates using primarily rapid quench and stopped-flow spectrophotometric methods. In addition, the sensitivity of the observed rate constants to both HPP ring deuterons and solvent-derived deuterons was observed, and these data were correlated with the effect on overall turnover from concurrent analyses in the steady state.

EXPERIMENTAL PROCEDURES

Materials. HPP, HG, glacial acetic acid, trichloroacetic acid, pyridoxal 5′-phosphate, L-tyrosine, 99.99 atom % deuterium oxide, and ferrous sulfate were purchased from ACROS. AKG, ampicillin, dithiothreitol, isopropyl β-thiogalactopyranoside (IPTG), and electrophoretic grade agarose were purchased from ICN Biomedicals Inc. Sodium hydroxide, HEPES buffer, HPLC grade acetonitrile, HPLC grade methanol, 2,3,5,6-tetradeuterio-L-tyrosine, and monobasic and dibasic sodium phosphate were from Sigma-Aldrich Chemical Co. The analytical Xterra reverse-phase (C18) (4.6 × 50 mm) column was from Waters. The preparative reverse-phase column (phenyl) (250 × 21.2 mm) was purchased from Phenomenex. Biomax 10 kDa centrifugal filters were from Amicon. *Nde*I and *Bam*HI restriction enzymes and T4 ligase were from New England Biolabs. Enzyme grade ammonium sulfate was purchased from Fisher. LB broth and LB agar were from BIO 101, Inc. The Macro-Prep DEAE anion-exchange column packing was from Bio-Rad. Oligonucleotides and the genomic tip DNA isolation kit were purchased from Qiagen. *PfuTURBO* DNA polymerase and TOP10 *Escherichia coli* cells were bought from Stratagene. The pET17b plasmid was from Novagen. BL21 DE3 *E. coli* were from Invitrogen.

Extinction Coefficients and Quantification. The extinction coefficient used for HPPD was as previously published (*9*). The extinction coefficient for HPP was determined using nuclear magnetic resonance and spectrophotometry. A solution of HPP in deuterium oxide (∼7 mM by weight) was prepared and its absorbance measured. This solution was then mixed with a 19 mM solution of tryptophan, also in deuterium oxide, in a 1:1 ratio. The aromatic resonances of tryptophan were used as an internal integration standard for the aromatic HPP resonances to determine the concentration of the original solution and hence the extinction coefficient of HPP. Using this method the extinction coefficient of HPP at equilibrium of the keto, enol, and diol forms at 276 nm was found to be 3400 M^{-1} cm^{-1} at pH 7.0. Dissolved oxygen concentration was controlled by sparging solutions for 10 min with blended ratios of nitrogen and oxygen gases supplied from a MAXblend Maxtec gas mixer with an in-line oxygen sensor coupled to a Timeter low-volume flow tube. The concentration of oxygen was confirmed using a calibrated Hansetech oxygen electrode. All other reagent concentrations were defined by weight.

Preparation of (4-Hydroxyphenyl)pyruvate Dioxygenase. HPPD was purified according to previously published methods (*9*). Unless otherwise stated all enzyme manipulations were undertaken at or below 5 °C. For pre-steady-state experiments in buffered deuterium oxide solution (pD = 7.0), the HPPD solvent was exchanged using repeated centrifugal concentration with a Millipore 10 kDa filter device and subsequent dilution. To ensure that this exchange procedure did not alter the sample significantly from other enzyme samples, all enzyme samples were prepared in a procedurally equivalent manner as follows: HPPD (24 mL of ∼60 μM) was thawed on ice and concentrated to approximately 500 μL. The sample was then diluted in 10 mL of 20 mM HEPES, pH (or pD) 7.0, and concentrated again to ∼500 μL. Each sample was then diluted to ∼3 mL in their respective buffered solvents and used immediately.

Cloning, Expression, and Purification of Tyrosine Aminotransferase and Preparation of Proteo- and 2,3,5,6-Tetradeuterio-(4-hydroxyphenyl)pyruvate. E. coli tyrosine aminotransferase (TAT) was used to synthesize proteo and 2,3,5,6-tetradeuterio ring-substituted HPP from L-tyrosine and 2,3,5,6-tetradeuterio-L-tyrosine, respectively. The gene for the TAT enzyme was cloned using standard PCR amplification and cloning protocols. The TAT enzyme was purified using ammonium sulfate fractionation and anion-exchange chromatography (see Supporting Information).

Anaerobic Preparation of the HPPD·Fe(II)·HPP Complex. The HPPD solution was placed in a tonometer. Sufficient HPP was placed in the sidearm of the tonometer to yield a saturating concentration of free HPP after the completion of a single turnover based on the previously measured dissociation constant for the HPPD·Fe(II)·HPP complex (>400 μM unbound HPP final concentration after single turnover) (*9*). Ferrous sulfate (∼1 mol equiv relative to HPPD) was added to another sidearm. The sample was then made anaerobic by 45 alternating vacuum and argon gas cycles (after each set of three cycles the sample was left to exchange dissolved gases for approximately 2 min). The apoenzyme−substrate mixture was then mixed initially with Fe(II) from the sidearm of the tonometer and then with HPP from the other sidearm.

Scheme 2

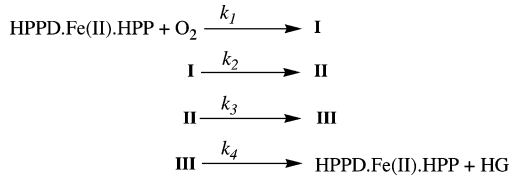

The anaerobic HPPD·Fe(II)·HPP complex had a characteristic burgundy color from a metal to α-keto acid ligand charge transfer band at around 500 nm.

Rapid Quench Single Turnover Product Analysis. The percentage of active HPPD was measured using an Update Instruments System 1000 chemical/freeze quench apparatus modified with an anaerobic sample mounting manifold and high-pressure valves to permit cleaning and flushing of age loops between quench reactions. Anaerobic HPPD·Fe(II)·HPP [462 μM final concentration; 480 μM HPPD, 462 μM Fe(II), 1.925 mM HPP] was prepared in a tonometer as described above and mixed against oxygenated buffer (454 μM final concentration) at 5 °C. The reaction was quenched in 3% trichloroacetic acid after specified age times. The age times were calibrated using the standard reaction of dinitrophenylacetate with hydroxide ion (*25*). This external acid quench method allows accurate quench times to a minimum of ~100 ms, limited by the capacity of the rapidly moving exiting solution to fully mix with the stationary acidic quench solution. The quenched reaction was spun for 10 min at 14000 rpm to pellet the precipitated protein, and the supernatant was injected onto an HPLC Phenomenex Synergi Phenyl column (250 × 4.6 mm) with a running buffer of 20 mM sodium citrate, pH 3.5, and the absorbance was monitored at 280 nm. The concentration of homogentisate at each age time was determined by comparison to a standard curve prepared from homogentisate that spanned the range 7−475 μM. Two reactions were quenched and analyzed for each time point and averaged.

Spectrophotometric Pre-Steady-State Analysis. All pre-steady-state spectrophotometric data were collected using a HiTech Scientific DX2 stopped-flow spectrophotometer. With the exception of fluorescence experiments, all reactant stoichiometries were pseudo first order with respect to the enzyme concentration. The HPPD·Fe(II)·HPP complex (~1.0 mM after mixing) was mixed versus a substoichiometric concentration of oxygen (~0.1 mM after mixing) at 5 °C, and the reaction was monitored for ≤20 s at all wavelengths between 300 and 700 nm using a photodiode array detection device and also at 380 and 490 nm using a photomultiplier tube. The latter detection method was used to maximize time resolution for accurate measurement of rate constants. Data obtained were analyzed using Specfit (Specsoft). Data were fit to the model depicted in Scheme 2, in which three intermediates accumulate in consecutive irreversible steps, and the free enzyme rapidly reacquires available HPP after the completion of turnover and the release of product, HG, via k_4. The t_{zero} and t_{end} spectra are thus equivalent between 420 and 600 nm due to metal-to-substrate−ligand charge transfer. Scheme 2 ignores the CO_2 product of HPPD as no evidence from the experiments conducted is indicative of in what step this product dissociates.

In fluorescence experiments the HPPD·Fe(II)·HPP complex was mixed versus stoichiometric concentrations (>9/10) of oxygen at 5 °C, and the reaction was monitored for ≤20 s. This reactant stoichiometry was used to maximize the fluorescence signal in the presence of a significant incident light inner filter from HPPD and HPP. Initially, the emission spectra for HPP and HG were measured using a Hitachi F-4500 fluorescence spectrophotometer. The product, HG, is approximately 15-fold more fluorescent than the substrate, HPP, when excited between 290 and 310 nm. The excitation maximum for HG is 290 nm; however, the fluorescence was monitored with 305 nm incident light again to reduce the combined effects of the HPPD and HPP inner filters. Total emission was measured by placing a 320 nm cutoff filter inline to a photomultiplier oriented 90 deg to the incident light. Individual fluorescence traces were also fit to the kinetic model depicted in Scheme 2 using Specfit (Specsoft Software).

Steady-State Kinetic Analyses of HPPD. Steady-state analyses of HPPD using proteo-HPP, 2,3,5,6-tetradeutero-HPP, and proteo-HPP in deuterium oxide were carried out in 1 mL assays on a Hansetech oxygen electrode. HPP solutions were prepared from the enzymatically synthesized HPP stocks with final concentrations ranging from 4 μM to 1 mM in 20 mM HEPES at pH (pD) 7.0. The assay mixture included ferrous sulfate (10 μM), DTT (1 mM), HPPD (500 nM), and HPP (0−1 mM) in 20 mM HEPES, pH (pD) 7.0, under conditions of atmospheric oxygen (350 μM at 5 °C). The reaction was initiated with HPP, and the turnover rate was determined from the first 20 s of oxygen consumption. These initial rates were plotted versus HPP concentration and analyzed for kinetic constants by fitting to the Michaelis−Menten equation using KaleidaGraph software (Versaterm Software).

Evidence of Homogentisate Complexation with HPPD·Fe(II). Spectophotometric evidence for an HPPD·Fe(II)·HG complex was sought by preparing HPPD (475 μM) with ferrous sulfate (450 μM) anaerobically in a tonometer as above. A stock of HG was prepared in 5 mM HCl. HG solutions (4 μM to 8 mM before mixing) were then made anaerobic by sparging with argon for 10 min in an inverted glass syringe. HG was mixed anaerobically versus HPPD·Fe(II) at 4 °C, and the spectrum was observed between 300 and 700 nm.

Steady-state evidence for the HPPD·Fe(II)·HG complex formation was also obtained from the observation of the extent of inhibition of HPPD by HG in the steady state. These experiments were carried out on a Hansetech oxygen electrode apparatus. Each 2 mL assay included HPPD (120 nM), ferrous sulfate (10 μM), HPP (30 μM and 250 μM), DTT (1 mM), and HG (varied from 50 μM to 3.2 mM) in 20 mM HEPES, pH 7.0. Each assay was performed at 25 °C and initiated with HPP.

RESULTS

Rapid Quench, Single Turnover Product Analysis. Rapid acid quench followed by HPLC product analysis was used to measure the fraction of active HPPD and to verify that our pre-steady-state methods yield a single turnover. The anaerobic HPPD·Fe(II)·HPP complex (462 μM) was mixed with an equivalent concentration of molecular oxygen, and the reaction was quenched at times between 115 ms and 6 s (Figure 1). Only the reaction quenched at 115 ms has a

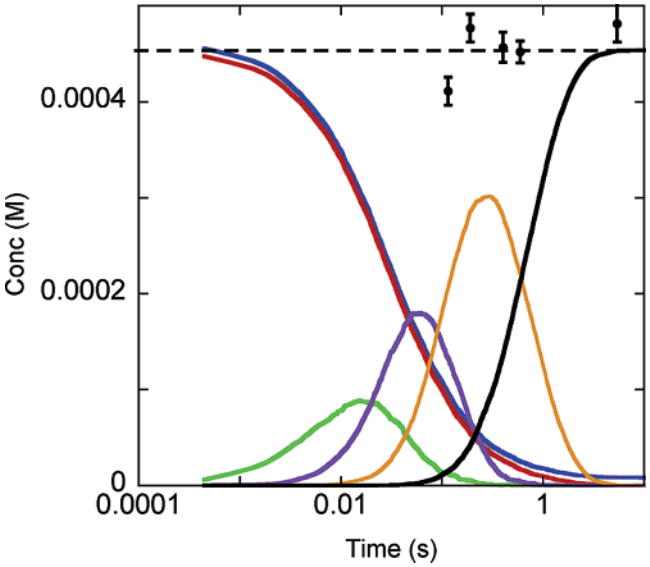

FIGURE 1: Acid quench and the fraction of active enzyme. Anaerobic HPPD·Fe(II)·HPP [462 μM final concentration; 480 μM HPPD, 462 μM Fe(II), 1.925 mM HPP] was prepared anaerobically and mixed against oxygenated buffer (454 μM final concentration) at 5 °C. The reaction was quenched in 3% trichloroacetic acid at the indicated age times. The quenched reaction was centrifuged for 10 min at 14000 rpm to pellet the precipitated protein, the supernatant was injected onto an HPLC Phenomenex Synergi Phenyl column (250 × 4.6 mm) with a running buffer of 20 mM sodium citrate, pH 3.5, and the absorbance was monitored at 280 nm. The concentration of homogentisate at each age time was determined by comparison to a standard curve. Two reactions were run at each time point and averaged. The dashed line represents 100% product formation. A simulation of the fractional accumulation of all species based on the concentrations used and the rate constants measured in subsequent experiments ($k_1 = 7.4 \times 10^4$ M^{-1} s^{-1}, $k_2 = 76$ s^{-1}, $k_3 = 13$ s^{-1}, and $k_4 = 1.6$ s^{-1}) is included. These species include HPPD·Fe(II)·HPP (blue), molecular oxygen (red), intermediate I (green), intermediate II (violet), and intermediate III (orange), and the black line represents the limiting rate constant of turnover corresponding to the re-formation of HPPD·Fe(II)·HPP and release of homogentisate.

percentage of HG product formation that is significantly less than stoichiometric with the initial enzyme−substrate complex (88%). The average of data points that were quenched at or greater than 191 ms is 466 ± 14 μM HG; this is within 1% of that expected for a stoichiometric single turnover (shown as a dashed black line in Figure 1). The data indicate that the HG product is formed during one turnover, as the amount of product is equivalent to the enzyme−substrate complex at 191 ms and does not increase in the time frame that a second catalytic event would be expected to proceed, based on the turnover number (1.6 s^{-1}, shown as a solid black line in Figure 1). All processes of the first turnover should be complete by approximately 2.5 s (5 half-lives of the limiting rate constant). Moreover, the data suggest that either HG is formed on the enzyme by ~200 ms or an intermediate species that rearranges to HG in the absence of HPPD predominates in the turnover reaction at this time. Collectively, these data verify that the HPPD as isolated is fully active and that intermediate extinction coefficients derived from spectrophotometric rapid mixing methods are characteristic of the reaction.

Pre-Steady-State Kinetic Analysis. Single turnover kinetics for HPPD were observed spectrophotometrically by mixing equal volumes of the anaerobic enzyme−substrate complex and solutions containing molecular oxygen in the presence of saturating HPP using a stopped-flow spectrophotometer. These experiments were carried out using either pseudo-first-order or stoichiometric reactant concentrations. For all absorbance data the observed amplitude changes scale proportionally to the enzyme concentration. For both the fluorescence and absorbance data no significant amplitude changes are observed in the absence of either the enzyme or the substrate (data not shown).

Due primarily to small changes in the extinction coefficient, it was necessary to use relatively large concentrations of enzyme to obtain suitable signal-to-noise ratios for the absorbance changes associated with the formation and decay of each intermediate. Enzyme−substrate complex in excess of molecular oxygen was used to establish pseudo-first-order conditions and, in addition, avoid the complexities of multiple turnovers that would arise in excess dioxygen. Such experiments, however, have relatively long mixing times due to the significant difference in viscosity of the reactant solutions. Thus experiments in which ~100 μM oxygen was reacted with ~1 mM enzyme (final concentrations) were conducted as a reasonable compromise between mixing time (6 ms), acceptable signal-to-noise ratio (~90:1), and the observed magnitude of the second-order rate constant, k_1. Approximately 50% of the first phase was obscured by light scatter that occurred during mixing. For this reason, data collected prior to 0.006 s were excluded from the analyses. The data obtained could be best fit to four first-order processes; the quality of the fit to the data and the degree of accumulation of the derived intermediates are shown in Figure 2. For each experiment an additional slow phase outside the realm of turnover was included (~0.3 s^{-1}) that corresponded to a small increase at all wavelengths. The amplitude of this phase varied slightly between experiments, and the origin of it is not known.

The rate constants derived from the fit to were $k_1 = (7.4 \pm 1.2) \times 10^4$ M^{-1} s^{-1}, $k_2 = 74 \pm 15$ s^{-1}, $k_3 = 13.2 \pm 0.3$ s^{-1}, and $k_4 = 1.60 \pm 0.13$ s^{-1}, indicating the accumulation of three catalytic intermediates. The deconvoluted pure intermediate spectra are shown in Figure 3. Intermediate I had the most intense absorbance spectrum with maxima at 370 and 480 nm with extinction coefficients of 2400 and 700 M^{-1} cm^{-1}, respectively. Intermediate II has a spectrum that is considerably less intense than intermediate I, having shoulders at 370 and 480 nm with respective extinction coefficients of 550 and 280 M^{-1} cm^{-1}. The spectrum of intermediate II is very similar to that of the t_{end} spectrum. Intermediate III is less intense than either the t_{zero} or t_{end} spectra, and the decay of III is observed as a minor increase in absorbance (average $\Delta\epsilon$ = 50−200 M^{-1} cm^{-1}) at all wavelengths monitored. This phase is concomitant with reacquisition of substrate as observed by the re-formation of the metal-to-ligand charge transfer of the HPPD·FeII·HPP complex between 420 and 700 nm (*9*, *26*). The conclusion from this observation is that the product, HG, is released and the substrate, HPP, is reacquired during the last phase observed (k_4).

During turnover by HPPD, aromatic oxygenation of the HPP phenol causes the decarboxylated α-ketopropionate side chain to shift to the adjacent carbon of the phenol, displacing one of the ortho protons (*27*, *28*). Substrate substituted with deuterons for aromatic protons was synthesized to test if

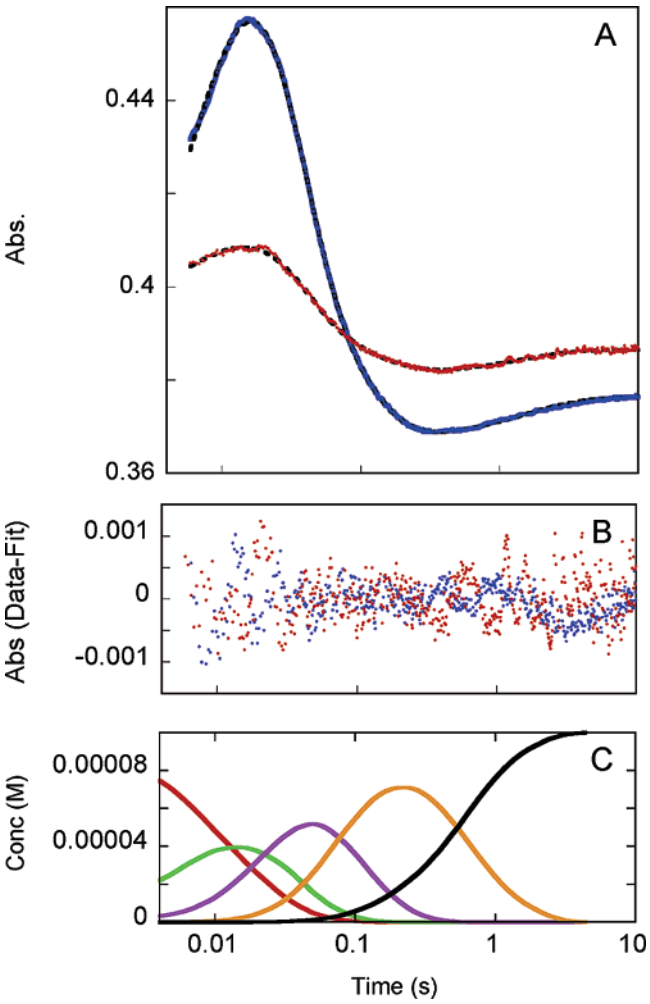

FIGURE 2: Kinetic data and fit using pseudo-first-order reactant stoichiometry in the presence of saturating HPP. The figure depicts the reaction of the HPPD·Fe(II)·HPP complex [1.0 mM HPPD, 1.0 mM Fe(II), and 1.5 mM HPP] with 100 μM molecular oxygen at pH 7.0 and 5 °C. (A) Stopped-flow traces observed at 380 nm (blue) and 490 nm (red) overlaying the fit (---) to the model described in Scheme 2 for the rate constants $k_1 = (7.2 \pm 1.15) \times 10^4$ M^{-1} s^{-1}, $k_2 = 74 \pm 15$ s^{-1}, $k_3 = 13.2 \pm 0.3$ s^{-1}, and $k_4 = 1.6 \pm 0.13$ s^{-1}. (B) Residuals of each trace in (A) (data minus the fit) to that trace in colors respective for each wavelength. (C) Fractional accumulation of species based on the reactant concentrations and rate constants described above: intermediate I (green), intermediate II (violet), intermediate III (orange), and HPPD·Fe(II)·HPP + HG (black). (For clarity, the enzyme−substrate complex is not depicted due to its order of magnitude higher concentration.)

processes of aromatic oxygenation to form homogentisate are among the observed pre-steady-state events. This substrate was placed in complex with HPPD and mixed with a limiting concentration of molecular oxygen as above. The kinetic data observed with this substrate are not significantly different from those observed with the proteo substrate (Figure 4). The traces at all wavelengths exhibit similar total amplitude changes compared to those observed with proteo-HPP. The fit of the data from this experiment indicated that three intermediates were also observed and these accumulated and decayed with comparable rate constants, $k_1 = (7.4 \pm 4.5) \times 10^4$ M^{-1} s^{-1}, $k_2 = 56 \pm 15$ s^{-1}, $k_3 = 7.6 \pm 0.3$ s^{-1}, and $k_4 = 1.54 \pm 0.04$ s^{-1}, to yield similar intermediate spectra. These data suggest that catalytic steps involved directly in the hydroxylation of the aromatic ring are among those observed. The kinetic isotope effect associated with

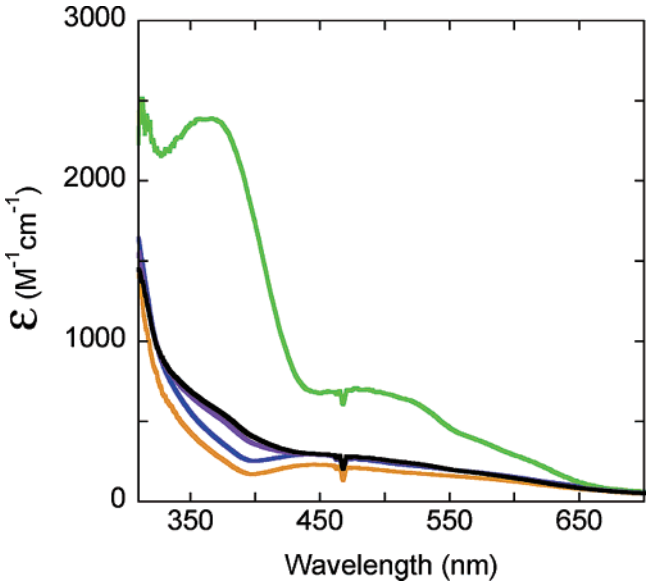

FIGURE 3: Intermediate spectra: HPPD·Fe(II)·HPP (blue), intermediate I (green), intermediate II (violet), intermediate III (orange), and HPPD·Fe(II)·HPP + HG + CO_2 (black).

k_3 (1.7) is, however, the only effect to have a magnitude greater than combined error.

The involvement of solvent-derived protons in the formation or decay of any of the observed intermediates was tested by exchanging the enzyme into buffered deuterium oxide and repeating the pre-steady-state analysis as described above. The shape of the derived intermediate spectra showed no significant influence of deuterated solvent, indicating that the exchange of displaceable protons for deuterons did not unveil otherwise kinetically unresolved intermediates. From the fit to the data, it was observed that the rate constants k_1, k_2, and k_3 were not significantly different from those determined from the experiment in H_2O ($k_1 = 7.4 \times 10^4 \pm 4.4 \times 10^3$ M^{-1} s^{-1}, $k_2 = 47 \pm 9$ s^{-1}, $k_3 = 15.4 \pm 3.5$ s^{-1}). These results suggest that protons derived from the solvent are not in flight during the formation or decay of intermediates I or II (Figure 5). The final phase in catalysis (k_4), however, decreased to 0.70 ± 0.04 s^{-1} in the presence of deuterium oxide solvent (a kinetic isotope effect of 2.2), indicating the involvement of a solvent-derived proton in this step (cf. Figures 2A and 5A).

The formation of the product can be monitored by fluorescence as HG is 15-fold more fluorescent than the substrate when excited at wavelengths around 300 nm (Figure 6A). To confirm the formation of HG in k_3, the anaerobic HPPD·Fe(II)·HPP complex was mixed with an equal concentration of molecular oxygen and excited using 305 nm light. Multiphasic fluorescence changes were observed (Figure 6B). The net amplitude change was positive, consistent with the formation of homogentisate. The amplitude associated with the first process, k_1, was too small to be accurately fit for the determination of a rate constant, indicating either that the first intermediate is nonfluorescent or that the net emission under the conditions of the experiment during this time was close to zero. The rate constant for this phase (or lag) was fixed to the rate constant observed for this process in absorbance experiments (7.4×10^4 M^{-1} s^{-1}). Similarly, the second phase observed was a small decrease in fluorescence that was fixed to 74 s^{-1}. The largest amplitude change

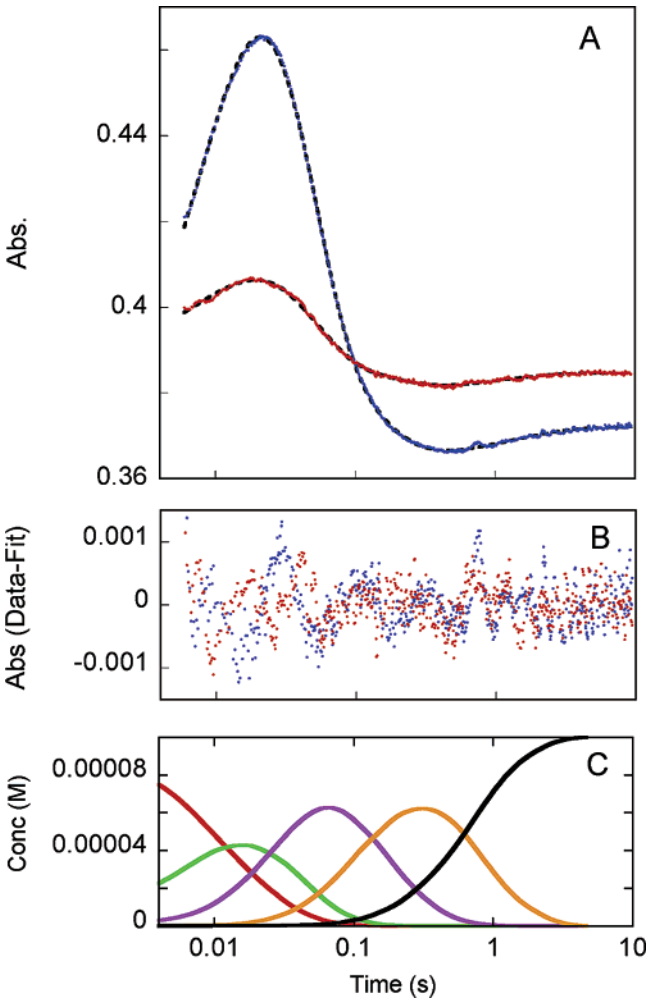

FIGURE 4: Intermediate spectra derived from pseudo-first-order reactant stoichiometry in the presence of saturating ring deuterated HPP. The figure depicts the reaction of the HPPD·Fe(II)·HPP complex [1.0 mM HPPD, 1.0 mM Fe(II) and 1.5 mM HPP] with 107 μM molecular oxygen at pH 7.0 and 5 °C. (A) Stopped-flow traces observed at 380 nm (blue) and 490 nm (red) overlaying the fit (---) to the model described in Scheme 2 for the rate constants $k_1 = (7.4 \pm 4.5) \times 10^4$ M^{-1} s^{-1}, $k_2 = 56 \pm 15$ s^{-1}, $k_3 = 7.6 \pm 0.3$ s^{-1}, and $k_4 = 1.54 \pm 0.04$ s^{-1}. (B) Residuals of each trace in (A) (data minus the fit) to that trace in colors respective for each wavelength. (C) Fractional accumulation of species based on the rate constants described above: intermediate I (green), intermediate II (violet), intermediate III (orange), and HPPD·Fe(II)·HPP + HG + CO_2 (black). (For clarity, the enzyme−substrate complex is not depicted due to its order of magnitude higher concentration.)

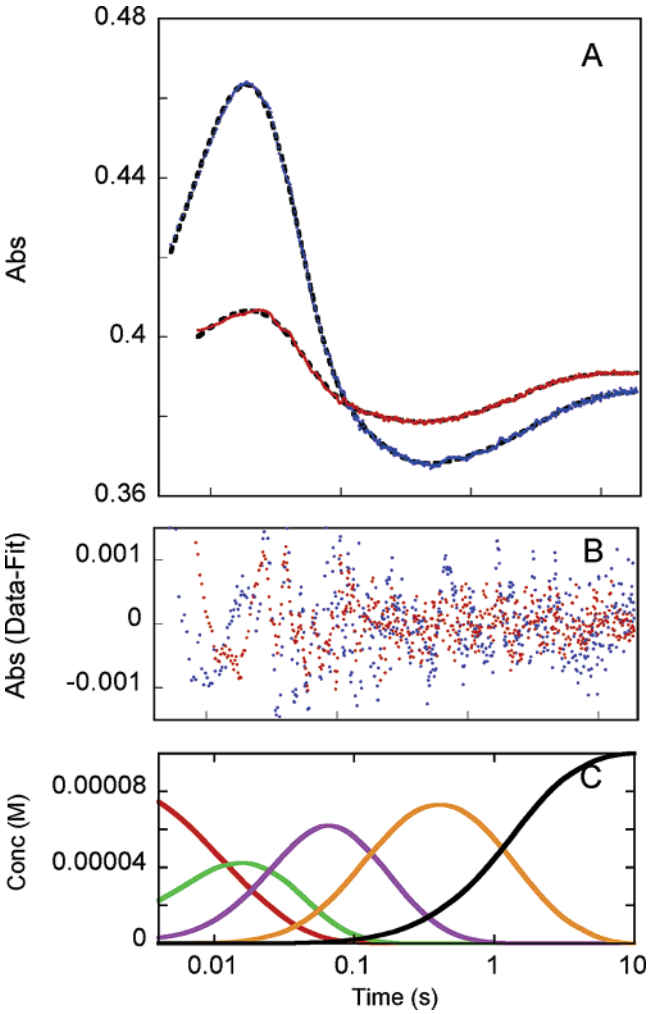

FIGURE 5: Intermediate spectra derived from pseudo-first-order reactant stoichiometry in the presence of 95% deuterium oxide solvent. The figure depicts the reaction of the HPPD·Fe(II)·HPP complex [1.0 mM HPPD, 1.0 mM Fe(II), and 1.5 mM HPP] with 101 μM molecular oxygen at pH 7.0 and 5 °C. (A) Stopped-flow traces observed at 380 nm (blue) and 490 nm (red) overlaying the fit (---) to the model described in Scheme 2 for the rate constants $k_1 = 7.4 \times 10^4 \pm 4.4 \times 10^3$ M^{-1} s^{-1}, $k_2 = 47 \pm 9$ s^{-1}, $k_3 = 15.4 \pm 3.5$ s^{-1}, and $k_4 = 0.70 \pm 0.04$ s^{-1}. (B) Residuals of each trace in (A) (data minus the fit) to that trace in colors respective for each wavelength. (C) Fractional accumulation of species based on the rate constants described above: intermediate I (green), intermediate II (violet), intermediate III (orange), and HPPD·Fe(II)·HPP + HG + CO_2 (black). (For clarity, the enzyme−substrate complex is not depicted due to its order of magnitude higher concentration.)

was an increase in fluorescence that corresponded to k_3 (15.3 ± 0.2 s^{-1}), consistent with homogentisate being formed during the third observable step in absorbance experiments (Figure 6B). The rate constant observed for this step in the presence of ring deuterio-HPP was 7.8 ± 0.3 (KIE = 1.9), consistent with the isotope effect observed in absorbance experiments (Figure 6B). No significant change was observed for the rate constant k_3 derived from fluorescence data with D_2O as a solvent.

Steady-State Kinetic Analysis. Steady-state kinetic analyses were undertaken at the same pH and temperature as single turnover experiments to evaluate whether the observations made in the pre-steady-state were observed in overall turnover. These experiments were undertaken in the presence of ring proteo-HPP, ring deutero-HPP, and deuterium oxide solvent (Table 1). For the native proteo substrate, the limiting value for the turnover number measured in water was 1.9 ± 0.1 s^{-1} and with ring deutero-HPP not significantly different (1.8 ± 0.1 s^{-1}). Moreover, the lack of a significant effect on *V*/*K* with this substrate is evidence that catalytic steps prior to the reduction of molecular oxygen are not kinetically sensitive to ring-derived deuterons.

The deuterium solvent isotope effect on the turnover number under these conditions was 2.6 ± 0.9, consistent with the primary rate-limiting process, k_4, being the only observable catalytic step in pre-steady-state experiments that exhibits a significant change in rate constant in this solvent. This indicates that a proton(s) derived from the solvent is (are) in flight in the release of the homogentisate product from the enzyme. The 5-fold decrease in the *V*/*K* value for HPP in D_2O is, however, unexpected and not clearly

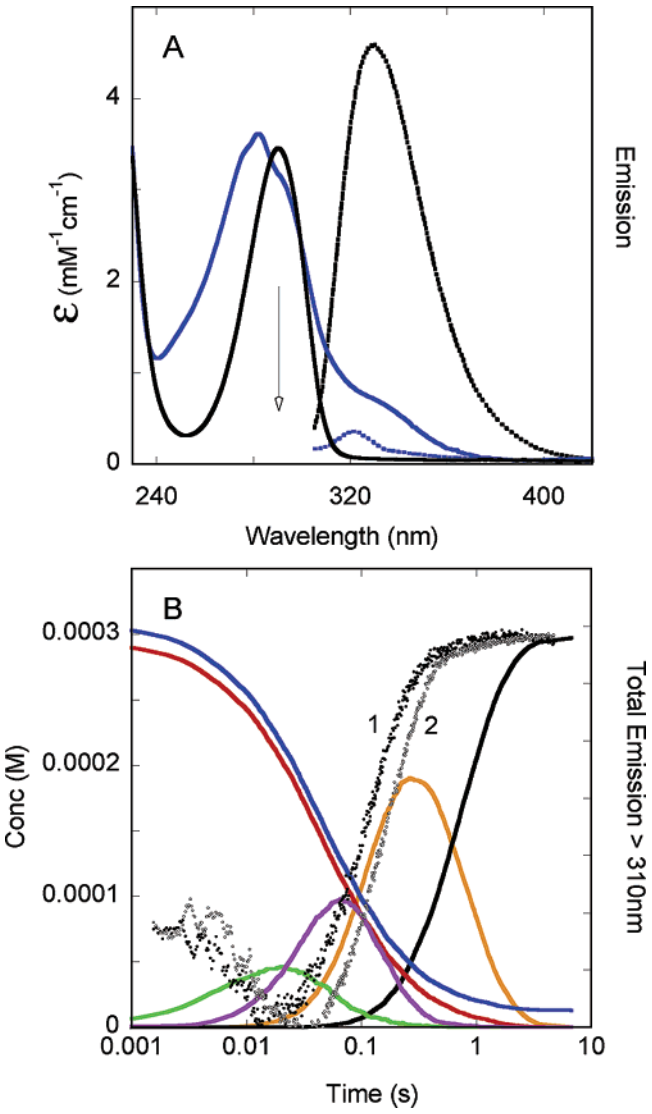

FIGURE 6: Stopped-flowed trace of total emission beyond 320 nm when excited with incident light of 305 nm for the reaction of the HPPD·Fe(II)·HPP complex with molecular oxygen at pH 7.0 and 5 °C. (A) Spectral characteristics of HPP (blue) and HG (black). Emission spectra from excitation at 290 nm (depicted by arrow) for each are shown with dashed lines. (B) Trace 1 is for 320 μM HPPD, 310 μM Fe(II), 950 μM HPP, and 297 μM molecular oxygen; trace 2 is for 320 μM HPPD, 310 μM Fe(II), 950 μM 2,3,5,6-tetradeuterio-HPP, and 281 μM molecular oxygen. A simulation of the fractional accumulation of all species based on the concentrations used and the rate constants measured in absorbance experiments with the nonisotopically substrate under pseudo-first-order conditions is included. These species include HPPD·Fe(II)·HPP (blue), molecular oxygen (red), intermediate I (green), intermediate II (violet), intermediate III (orange), and HPPD·Fe(II)·HPP + HG (black).

reconcilable with the pre-steady-state observations. This value suggests that a process prior to the irreversible reduction of molecular oxygen is affected by the presence of solvent-derived deuterons. However, this value is somewhat less accurately known due to insensitivity of the oxygen electrode relative to these quite low average turnover rates in the *V*/*K* substrate concentration range as is evidenced from the relatively high error in this value.

HG Complexation. Collectively, the results from quench experiments, the re-formation of the HPPD·Fe(II)·HPP charge transfer complex with the decay of intermediate III, and the concomitant increase in fluoresecence observed imply that intermediate III is a complex of the enzyme and the product, HG. To determine if a reversible association with the product occurs, the anaerobic HPPD·Fe(II) complex was mixed with a range of concentrations of anaerobic HG (4 μM to 8 mM), and the spectrophotometric changes were recorded. These data show no charge transfer or other evidence of product complexation with the free enzyme. To further verify the lack of reversible product complex, HG was assessed as an inhibitor of steady-state turnover. Concentrations of HG from 50 μM to 3.2 mM produced no effect on the values of V_{max} or *V*/*K*, clearly establishing that the release of product from the enzyme is irreversible and implying that the apparent product complex observed in the pre-steady state involves an otherwise energetically inaccessible conformation of the active site.

DISCUSSION

Recently, an intermediate was observed to accumulate in the reaction of the HPPD−substrate complex with molecular oxygen (*9*). Here we have expanded upon these observations by undertaking multiwavelength pre-steady-state analyses using the native substrate, ring deuterium labeled substrate, and deuterium oxide solvent. These data have been correlated with steady-state investigations to verify the pre-steady-state observations in relation to rate-limiting steps. Together, these observations serve as a prelude to a rapid freeze quench investigation to chemically characterize observed intermediate species by other spectroscopies.

The chemical characterization of reaction coordinate intermediates is the current frontier of enzyme chemistry. Generally, identification of enzyme-bound intermediates requires trapping of the transients from the liquid state for the application of a number of specific spectroscopies or analytical methods. Freezing in the crystal state with stepwise advancement of the reaction by controlling temperature and X-ray structural analysis (*16*, *22*−*24*, *29*) is also employed. For these approaches, the various steps in the reaction are often not well delineated with the data acquired, and the captured reactions are generally mixtures of multiple accumulating and decaying transients that are not easily deconvoluted due to the limited time resolution provided from trapping methodologies. Other evidence for the magnitude of rate constants for individual catalytic steps facilitates interpretation of quench-derived data. Currently, rate constants are most accurately measured using spectrophotometric methods due to the relatively rapid integration time achieved and hence the large number of averaged data points obtained. Historically, spectrophotometric pre-steady-state analyses have been preferably conducted with enzymes that have strongly absorbing and/or fluorescing reporter groups such as hemes and flavins. Fe(II)-dependent non-heme enzymes have long been regarded as having no significant chromophores. Recently, however, a number of these enzymes have been shown to have weakly absorbing complexes and intermediates (*9*, *16*, *17*).

Pre-steady-state analyses are most definitive when conducted under pseudo-first-order conditions, i.e., where one of the reactants is in great excess. Under such conditions the integrated rate expression is simplified and individual reaction processes closely approximate pure first-order

Table 1: Steady-State Kinetic Analysis of HPPD

HPP	solvent	V_{max} (s^{-1})[a]	K_m (mM)[a]	V_{max}/K_m ($mM^{-1}\,s^{-1}$)	^DV[b]	$^DV/K$[c]
2,3,5,6-tetraproteo	H_2O	1.9 ± 0.1	22 ± 4	0.09 ± 0.01		
2,3,5,6-tetradeuterio	H_2O	1.8 ± 0.1	11 ± 2	0.15 ± 0.02	1.01 ± 0.1	0.72 ± 0.14
2,3,5,6-tetraproteo	D_2O	0.86 ± 0.1	54 ± 13	0.02 ± 0.01	2.6 ± 0.9	4.5 ± 2.3

[a] Steady-state analyses of HPPD using protonated HPP and 2,3,5,6-tetradeuterated and protonated HPP in deuterium oxide were carried out in a 1 mL assay on a Hansetech oxygen electrode at 5 °C. HPP solutions were prepared from the enzymatically synthesized HPP stocks with final concentrations ranging from 4 μM to 1 mM in 20 mM HEPES at pH (pD) 7.0. The assay mixture included ferrous sulfate (5 μM), DTT (1 mM), HPPD (100 nM), and HPP (0−1 mM) in 20 mM HEPES, pH (pD) 7.0, under conditions of atmospheric oxygen. The reaction was initiated with HPP, and the turnover rate was determined from the first 20 s of oxygen consumption. These initial rates were plotted versus HPP concentration and analyzed for kinetic constants by fitting to the Michealis−Menten equation using KaleidaGraph software (Versaterm Software). [b] The deuterium kinetic isotope effect for V_{max}. [c] The deuterium kinetic isotope effect for V_{max}/K_m.

events. A 10-fold excess of one of the reactants is the generally accepted minimum concentration ratio for pseudo-first-order reaction conditions. For an oxygenase enzyme with weakly absorbing static and transient species, pseudo-first-order conditions with respect to molecular oxygen are often not easily obtainable or, from the standpoint of analysis, desirable. The aqueous oxygen solubility ceiling of approximately 2 mM at 4 °C under atmospheric pressure dictates that the highest concentration available after symmetrical mixing with an anaerobic enzyme sample is ~1 mM, and thus to preserve pseudo-first-order conditions, the final enzyme concentration would be equal to or less than 100 μM. Reactant ratios such as these result in added complications that make the end point of a single turnover reaction unclear. The first of these is that the enzyme will conduct multiple turnovers; the second that is unique to Fe(II)-dependent enzymes is that the active site metal ion will typically oxidize to Fe(III) in the residual oxygen that remains after the consumption of the organic substrate, producing additional unique chromophores associated with this oxidation state.

An alternate approach that can achieve reasonable signal-to-noise ratios is to be pseudo-first order in the enzyme−substrate complex, as is the case here; however, this is an exceedingly expensive process requiring large concentrations of enzyme that produce the added complication of causing schlieren artifacts in mixing. However, under these reactant conditions, completion of a single turnover consumes all available oxygen and returns the enzyme to the anaerobic enzyme−substrate complex, halting both catalysis and subsequent oxidative processes and more clearly defining the spectrophotometric end point for the single turnover reaction.

Yet, another approach is the matched reactant concentration experiment. This has the advantage of permitting easy measurement of second-order rate constants though it is generally less interpretable due to the increased degree of reactant overlap with transients that occurs at any point in time (see simulations in Figures 1 and 6). The effects of this complication can be mitigated if transients form and decay with large descending differences in rate constant magnitude or have characteristics that provide sensitive unique detection (*21*). The latter of these conditions was utilized here for both external acid quench and fluorescence experiments.

External acid quench experiments followed by HG product analysis were designed to measure the fraction of active enzyme and thus verify that the pre-steady-state experiments involved a single turnover. The reaction achieves stoichiometric production of HG by 191 ms, indicating that either HG is formed on the enzyme by this time or high fractional accumulation of an intermediate species that decays in acid to yield HG is present. The stoichiometric production of HG in reactions quenched prior to the completion of a single turnover and the lack of subsequent higher accumulations of product indicate that the enzyme used was fully active.

Scheme 3

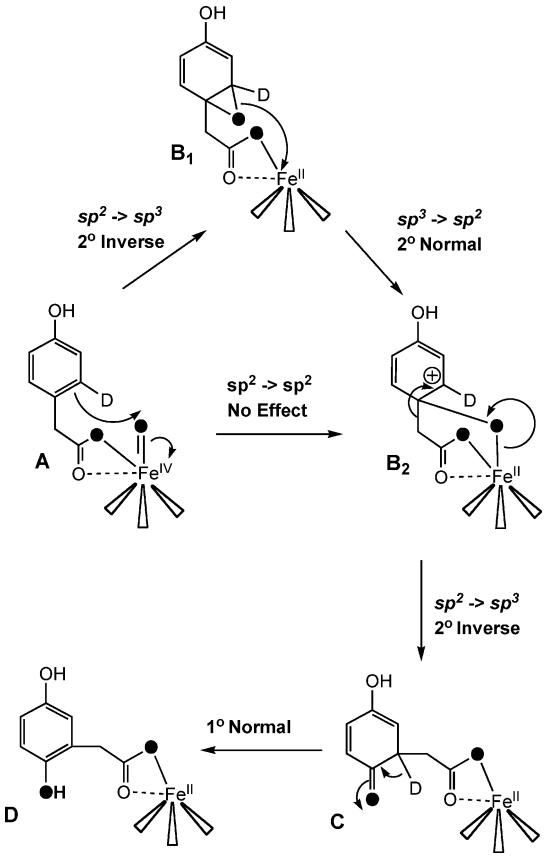

Pseudo-first-order reactant stoichiometry with respect to the HPPD·Fe(II)·HPP complex was employed for all absorbance-based kinetic experiments. These data provide the foundation for definitive interpretation of the non-pseudo-first-order, matched reactant concentration fluorescence and quench experiments. The data indicate that three spectrophotometrically observable intermediates accumulate during the course of a single turnover (Figures 2 and 3). The rate constant for each successive step allows significant accumulation of each transient (Figure 2C). Intermediate I had the lowest maximal accumulation at 14 ms of 40% of total species, while intermediate II had ~50% maximal accumula-

Scheme 4

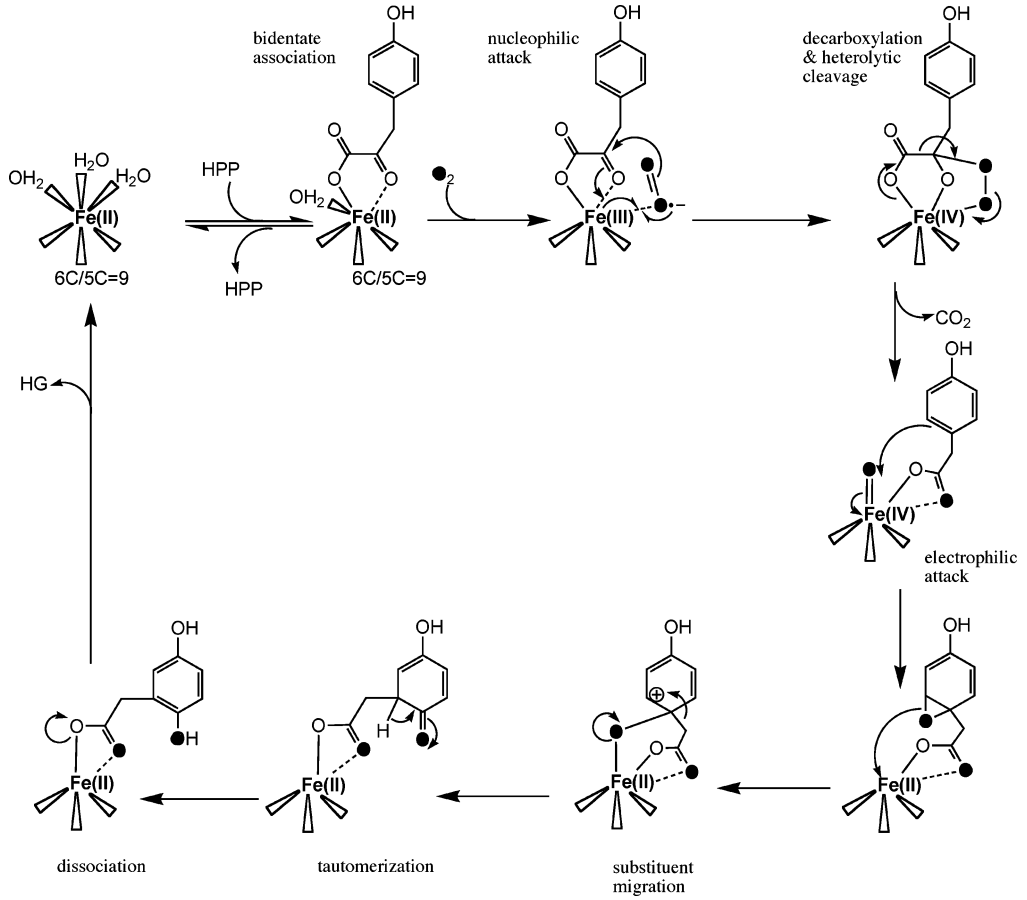

tion at 47 ms and intermediate III exhibited 70% accumulation at 220 ms. High fractional accumulations such as these bode well for ultimately trapping a significant concentration of these transients by the freeze quench technique.

While no direct evidence for the identity of intermediates is available from these experiments, a number of reasonable conclusions are supported by the data. The first observed phase of catalysis occurs via a second-order or collision-based process. The magnitude of the observed rate constant shows little variation between experiments and is best fit to a value in the 7.4×10^4 M^{-1} s^{-1} range, consistent with previous observations (*9*). The intermediate that accumulates from this process is the most strongly absorbing species observed in turnover, having extinction coefficient changes on the order of 2000 M^{-1} cm^{-1} at 370 nm. Given the fact that the rate of formation and decay of this species is not measurably influenced in the presence of substrate ring deuterons, it is tempting to conclude that intermediate I exists prior to aromatic hydroxylation. The obvious question is whether this intermediate is equivalent to an Fe(IV)−oxo intermediate, given that such an intermediate is the first observed to accumulate in TauD; all preceding processes of oxygen reduction and decarboxylation are assumed to be rapid (*16*). A number of Fe(IV)−oxo complexes have been isolated and characterized. These molecules tend to show weak extinction coefficient transitions (300−400 M^{-1} cm^{-1}) in the far-visible to near-IR region of the spectrum (*7*). To establish if such a transition exists for intermediate I, individual traces were recorded at 750 and 800 nm (the latter being the practical limit of the transmission spectrum of the tungsten lamp with the instrumentation employed). These traces showed no evidence of the development of long-wavelength transitions concomitant with the arrival of the first intermediate (data not shown).

In the reaction of HPPD, the aromatic oxygenation process induces an NIH shift that displaces an aceto substituent to the adjacent carbon of the aromatic ring (*27*). This hydroxylation is unique in nature as no other enzyme displaces an aromatic substituent of this size. Moreover, for other enzyme mechanisms that have been shown to involve an NIH shift, substituents at the point of oxygenation larger than a tritium are retained in the product in only a minor fraction of total catalysis (*30*, *31*). In the 40 years following the original observation the mechanism of the NIH shift has not reached consensus, particularly for the mononuclear non-heme iron oxygenases (*32*). The reason for this is that methods have not permitted researchers to clearly distinguish between aromatic oxygenation that yields an arene oxide or an arenium cation as the first intermediate after oxygen insertion. However, there has been a long-standing accord that the intermediate that precedes either the epoxide or cation is an oxy−ferryl, though until recently this apparent congruence was almost completely unsupported. On the strength of the studies of TauD, most investigators would now recognize that the oxygen atom used to hydroxylate the substrate in iron-dependent mononuclear non-heme oxygenases is, as suspected, provided by an oxo−ferryl intermediate (*16*, *22*−*24*). It is the preceding and subsequent steps that remain unresolved. The data offered here show that at least four catalytic steps are discernible in the catalytic cycle of HPPD, suggesting that this enzyme is a viable option from which to pursue evidence for these other processes.

For HPPD, the only evidence for either the arene oxide or cation has been the observation of a 1,2-epoxide product released from a mutant form of the enzyme (*8*). The pattern and magnitude of isotope effects that could arise from ring oxygenation in the presence of an ortho ring deuterium atom are conceivably one way to resolve the mechanism of the NIH shift and reveal the identity of intermediates that follow hydroxylation. A minimal hypothetical scheme for such events is depicted in Scheme 3. The small normal kinetic isotope effect on k_3 observed here in the presence of ring deuterons (Figures 4 and 6) indicates that processes of aromatic oxygenation are among those observed. Only the decay of arene oxide (B_1) or the dienone tautomer of the product (C) would be predicted to yield normal kinetic isotope effects in the presence of an ortho ring deuteron. The magnitude of this effect (1.7−1.9) is large for the secondary effect predicted for the decay of the epoxide and more likely to be a primary effect arising from the tautomerization of the dienone. The tentative assignment of intermediate II as C seems reasonable as the decay of this species involves a significant increase in fluorescence correlated with the appearance of product, HG (Figures 1 and 6).

Intermediate III decays with the re-formation of the substrate charge transfer bands by k_4. This suggests that intermediate III may be a complex of the product, HG, with the holoenzyme whose slow decay limits turnover by the product physically blocking access to the active site ($k_4 = 1.6\ s^{-1}$). This assertion is well supported by the acid quench experiments, the observation that the largest increase in fluorescence (due to the 15-fold more fluorescent HG product) is observed during the preceding step, k_3, and by the fact that no further changes in fluorescence are observed during the final phase, k_4 (Figure 6). The observed rate constant for k_4 is derived from a fit to a small absorbance increase at all wavelengths monitored. The value of the rate constant is sensitive to deuterium derived from the solvent. In 95% D_2O, a solvent kinetic isotope effect of 2 is observed in this phase, invoking a role for an active site base in product release (Figure 5, Table 1). Conceivably, this could involve protonation of either the product 2-hydroxyl or aceto groups to facilitate product release. If HG were able to dissociate and reassociate with the enzyme after turnover, complexation of the product with the free enzyme should be observed. However, even at millimolar concentrations no spectrophotometric perturbation or evidence of inhibitory response to HG in turnover is observed. Together, these observations indicate that HPPD undergoes rate-limiting conformational change(s) and proton movement during product release that leave the active site unable to rebind HG.

Scheme 4 depicts a tentative mechanistic hypothesis for HPPD compiled from a number of earlier observations, those described here, and those from other mechanistically related enzymes. In Scheme 4, catalysis is initiated by the bidentate association of the substrate to form a complex that displays a mixture of five- and six-coordinate geometry, whose overall coordination number is not altered from the free enzyme (*26*). This complex has elevated dioxygen reactivity (*9*, *33*) and delocalizes electron density from a planar α-keto acid moiety of the substrate to dioxygen (*20*), thereby denuding the substrate of electrons and inducing a nucleophilic attack at the pyruvate Cα atom. Dioxygen reduction is comprised of individual one-electron steps to satisfy the requirement for spin inversion in the two-electron reduction of the dioxygen ground state triplet. Attack at the pyruvate Cα atom yields an Fe(IV)-bridged peroxy species. Heterolytic cleavage of the peroxy bond occurs during decarboxylation to yield the highly electrophilic Fe(IV)−oxo intermediate (*16*, *18*, *34*) that can withdraw electrons from the aromatic ring inducing the formation of a 1,2-epoxide that then opens to the cation (*8*). The localization of the cation ortho to the aceto substituent would direct the shift of the side chain to form a dienone that need only tautomerize (k_3 here) to produce the product, HG, that dissociates slowly, limiting the turnover rate (k_4 here).

SUPPORTING INFORMATION AVAILABLE

2,3,5,6-Tetraproteo- and 2,3,5,6-tetradeuterio-HPP were enzymatically synthesized using tyrosine aminotransferase. The gene for this enzyme was cloned from *E. coli*, and simplified purification methods were developed for use in this synthetic protocol. The fractional conversion of tyrosine to HPP by TAT was studied by varying the tyrosine to α-ketoglutarate ratio in conjunction with HPP product analysis. This material is available free of charge via the Internet at http://pubs.acs.org.

REFERENCES

1. Lindstedt, S., Holme, E., Lock, E. A., Hjalmarson, O., and Strandvik, B. (1992) Treatment of hereditary tyrosinaemia type I by inhibition of 4-hydroxyphenylpyruvate dioxygenase, *Lancet 340*, 813−817.
2. Phornphutkul, C., Introne, W. J., Perry, M. B., Bernardini, I., Murphey, M. D., Fitzpatrick, D. L., Anderson, P. D., Huizing, M., Anikster, Y., Gerber, L. H., and Gahl, W. A. (2002) Natural history of alkaptonuria, *N. Engl. J. Med. 347*, 2111−2121.
3. Yang, C., Pflugrath, J. W., Camper, D. L., Foster, M. L., Pernich, D. J., and Walsh, T. A. (2004) Structural basis for herbicidal inhibitor selectivity revealed by comparison of crystal structures of plant and mammalian 4-hydroxyphenylpyruvate dioxygenases, *Biochemistry 43*, 10414−10423.
4. Brownlee, J., Kayunta, J.-W., Harrison, D. H. T., and Moran, G. R. (2004) The structure of the ferrous form of (4-hydroxyphenyl)-pyruvate dioxygenase from *Streptomyces avermitilis* in complex with the therapeutic herbicide, NTBC, *Biochemistry 43*, 6370−6377.
5. Solomon, E. I., Brunold, T. C., Davis, M. I., Kemsley, J. N., Lee, S. K., Lehnert, N., Neese, F., Skulan, A. J., Yang, Y. S., and Zhou, J. (2000) Geometric and electronic structure/function correlations in non-heme iron enzymes, *Chem. Rev. 100*, 235−350.
6. Hausinger, R. P. (2004) FeII/alpha-ketoglutarate-dependent hydroxylases and related enzymes, *Crit. Rev. Biochem. Mol. Biol. 39*, 21−68.
7. Costas, M., Mehn, M. P., Jensen, M. P., and Que, L. (2004) Dioxygen activation at mononuclear nonheme iron active sites: Enzymes, models, and intermediates, *Chem. Rev. 104*, 939−986.
8. Gunsior, M., Ravel, J., Challis, G. L., and Townsend, C. A. (2004) Engineering p-hydroxyphenylpyruvate dioxygenase to a p-hydroxymandelate synthase and evidence for the proposed benzene oxide intermediate in homogentisate formation, *Biochemistry 43*, 663−674.
9. Johnson-Winters, K., Purpero, V. M., Kavana, M., Nelson, T., and Moran, G. R. (2003) (4-Hydroxyphenyl)pyruvate dioxygenase from *Streptomyces avermitilis*: The basis for ordered substrate addition, *Biochemistry 42*, 2072−2080.
10. Holme, E. (1975) A kinetic study of thymine 7-hydroxylase from neurospora crassa, *Biochemistry 14*, 4999−5003.
11. Myllyla, R., Tuderman, L., and Kivirikko, K. I. (1977) Mechanism of the prolyl hydroxylase reaction. 2. Kinetic analysis of the reaction sequence, *Eur. J. Biochem. 80*, 349−357.

12. Tuderman, L., Myllyla, R., and Kivirikko, K. I. (1977) Mechanism of the prolyl hydroxylase reaction. 1. Role of co-substrates, *Eur. J. Biochem. 80*, 341−348.
13. Puistola, U., Turpeenniemi-Hujanen, T. M., Myllyla, R., and Kivirikko, K. I. (1980) Studies on the lysyl hydroxylase reaction. II. Inhibition kinetics and the reaction mechanism, *Biochim. Biophys. Acta 611*, 51−60.
14. De Carolis, E., and De Luca, V. (1993) Purification, characterization, and kinetic analysis of a 2-oxoglutarate-dependent dioxygenase involved in vindoline biosynthesis from *Catharanthus roseus*, *J. Biol. Chem. 268*, 5504−5511.
15. Elkins, J. M., Ryle, M. J., Clifton, I. J., Dunning Hotopp, J. C., Lloyd, J. S., Burzlaff, N. I., Baldwin, J. E., Hausinger, R. P., and Roach, P. L. (2002) X-ray crystal structure of *Escherichia coli* taurine/alpha-ketoglutarate dioxygenase complexed to ferrous iron and substrates, *Biochemistry 41*, 5185−5192.
16. Price, J. C., Barr, E. W., Tirupati, B., Bollinger, J. M., Jr., and Krebs, C. (2003) The first direct characterization of a high-valent iron intermediate in the reaction of an alpha-ketoglutarate-dependent dioxygenase: a high-spin FeIV complex in taurine/alpha-ketoglutarate dioxygenase (TauD) from *Escherichia coli*, *Biochemistry 42*, 7497−7508.
17. Ryle, M. J., Padmakumar, R., and Hausinger, R. P. (1999) Stopped-flow kinetic analysis of *Escherichia coli* taurine/alpha-ketoglutarate dioxygenase: interactions with alpha-ketoglutarate, taurine, and oxygen, *Biochemistry 38*, 15278−15286.
18. Borowski, T., Bassan, A., and Siegbahn, P. E. M. (2004) 4-Hydroxyphenylpyruvate dioxygenase: A hybrid density functional study of the catalytic reaction mechanism, *Biochemistry 43*, 12331−12342.
19. Valegard, K., van Scheltinga, A. C., Lloyd, M. D., Hara, T., Ramaswamy, S., Perrakis, A., Thompson, A., Lee, H. J., Baldwin, J. E., Schofield, C. J., Hajdu, J., and Andersson, I. (1998) Structure of a cephalosporin synthase, *Nature 394*, 805−809.
20. Pavel, E. G., Zhou, J., Busby, R. W., Gunsior, M., Townsend, C. A., and Solomon, E. I. (1998) Circular dichroism and magnetic circular dichroism spectroscopic studies of the non-heme ferrous active site in clavaminate synthase and its interaction with alpha-ketoglutarate cosubstrate, *J. Am. Chem. Soc. 120*, 743−753.
21. Grzyska, P. K., Ryle, M. J., Monterosso, G. R., Liu, J., Ballou, D. P., and Hausinger, R. P. (2005) Steady-state and transient kinetic analyses of taurine/-ketoglutarate dioxygenase: Effects of oxygen concentration, alternative sulfonates, and active-site variants on the FeIV-oxo intermediate, *Biochemistry* (in press).
22. Price, J. C., Barr, E. W., Glass, T. E., Krebs, C., and Bollinger, J. M., Jr. (2003) Evidence for hydrogen abstraction from C1 of taurine by the high-spin Fe(IV) intermediate detected during oxygen activation by taurine:alpha-ketoglutarate dioxygenase (TauD), *J. Am. Chem. Soc. 125*, 13008−13009.
23. Proshlyakov, D. A., Henshaw, T. F., Monterosso, G. R., Ryle, M. J., and Hausinger, R. P. (2004) Direct detection of oxygen intermediates in the non-heme Fe enzyme taurine/alpha-ketoglutarate dioxygenase, *J. Am. Chem. Soc. 126*, 1022−1023.
24. Riggs-Gelasco, P. J., Price, J. C., Guyer, R. B., Brehm, J. H., Barr, E. W., Bollinger, J. M., Jr., and Krebs, C. (2004) EXAFS spectroscopic evidence for an Fe=O unit in the Fe(IV) intermediate observed during oxygen activation by taurine:alpha-ketoglutarate dioxygenase, *J. Am. Chem. Soc. 126*, 8108−8109.
25. Gutfreund, H. (1969) Resolution of optical and sampling methods, *Methods Enzymol. 16*, 229−249.
26. Neidig, M. L., Kavana, M., Moran, G. R., and Solomon, E. I. (2004) CD and MCD studies of the non-heme ferrous active site in (4-hydroxyphenyl)pyruvate dioxygenase: Correlation between oxygen activation in the extradiol and alpha-KG dependent dioxygenases, *J. Am. Chem. Soc. 126*, 4486−4487.
27. Rundgren, M. (1982) Tritium isotope effects in the reaction catalyzed by 4-hydroxyphenylpyruvate dioxygenase from *Pseudomonas* sp. strain P.J. 874, *Biochim. Biophys. Acta 704*, 59−65.
28. Leinberger, R., Hull, W. E., Simon, H., and Retey, J. (1981) Steric course of the NIH shift in the enzymic formation of homogentisic acid, *Eur. J. Biochem. 117*, 311−318.
29. Schlichting, I., Berendzen, J., Chu, K., Stock, A. M., Maves, S. A., Benson, D. E., Sweet, R. M., Ringe, D., Petsko, G. A., and Sligar, S. G. (2000) The catalytic pathway of cytochrome p450cam at atomic resolution, *Science 287*, 1615−1622.
30. Hillas, P. J., and Fitzpatrick, P. F. (1996) A mechanism for hydroxylation by tyrosine hydroxylase based on partitioning of substituted phenylalanines, *Biochemistry 35*, 6969−6975.
31. Sono, M., Roach, M. P., Coulter, E. D., and Dawson, J. H. (1996) Heme-containing oxygenases, *Chem. Rev. 96*, 2841−2888.
32. Guroff, G., Daly, J. W., Jerina, D. M., Renson, J., Witkop, B., and Udenfriend, S. (1967) Hydroxylation-induced migration: The NIH shift, *Science 157*, 1524−1530.
33. Rundgren, M. (1977) Steady state kinetics of 4-hydroxyphenylpyruvate dioxygenase from human liver (III), *J. Biol. Chem. 252*, 5094−5099.
34. Borowski, T., Bassan, A., and Siegbahn, P. E. (2004) A hybrid density functional study of O−O bond cleavage and phenyl ring hydroxylation for a biomimetic non-heme iron complex, *Inorg. Chem. 43*, 3277−3291.

BI047625K